Genetics in Medicine (2022) 24, 439–453

ELSEVIER

Genetics in Medicine

www.journals.elsevier.com/genetics-in-medicine

ARTICLE

Loss-of-function variants in exon 4 of *TAB2* cause a recognizable multisystem disorder with cardiovascular, facial, cutaneous, and musculoskeletal involvement

Lucia Micale[1], Silvia Morlino[1], Annalucia Carbone[2], Annamaria Carissimo[3], Grazia Nardella[1], Carmela Fusco[1], Orazio Palumbo[1], Annalisa Schirizzi[1], Federica Russo[1], Gianluigi Mazzoccoli[2], Jeroen Breckpot[4], Chiara De Luca[4], Alessandro Ferraris[5], Cecilia Giunta[6], Paola Grammatico[5], Maria K. Haanpää[7], Giorgia Mancano[8], Giulia Forzano[9], Davide Cacchiarelli[10,11], Hilde Van Esch[4], Bert Callewaert[12], Marianne Rohrbach[6], Marco Castori[1,*]

ARTICLE INFO

Article history:
Received 23 July 2021
Revised 2 September 2021
Accepted 15 October 2021
Available online 30 November 2021

Keywords:
Congenital heart defect
Connective tissue
Ehlers-Danlos syndrome
Osteoblast
TAK1

ABSTRACT

Purpose: This study aimed to describe a multisystemic disorder featuring cardiovascular, facial, musculoskeletal, and cutaneous anomalies caused by heterozygous loss-of-function variants in *TAB2*.

Methods: Affected individuals were analyzed by next-generation technologies and genomic array. The presumed loss-of-function effect of identified variants was assessed by luciferase assay in cells transiently expressing *TAB2* deleterious alleles. In available patients' fibroblasts, variant pathogenicity was further explored by immunoblot and osteoblast differentiation assays. The transcriptomic profile of fibroblasts was investigated by RNA sequencing.

Results: A total of 11 individuals from 8 families were heterozygotes for a novel *TAB2* variant. In total, 7 variants were predicted to be null alleles and 1 was a missense change. An additional subject was heterozygous for a 52 kb microdeletion involving *TAB2* exons 1 to 3. Luciferase assay indicated a decreased transcriptional activation mediated by NF-κB signaling for all point variants. Immunoblot analysis showed a reduction of TAK1 phosphorylation while osteoblast differentiation was impaired. Transcriptomic analysis identified deregulation of multiple pleiotropic pathways, such as *TGFβ*-, *Ras-MAPK*-, and *Wnt*-signaling networks.

Conclusion: Our data defined a novel disorder associated with loss-of-function or, more rarely, hypomorphic alleles in a restricted linker region of *TAB2*. The pleiotropic manifestations in this disorder partly recapitulate the 6q25.1 (*TAB2*) microdeletion syndrome and deserve the definition of cardio-facial-cutaneous-articular syndrome.

Lucia Micale and Silvia Morlino contributed equally.

*Correspondence and requests for materials should be addressed to Marco Castori, Division of Medical Genetics, Fondazione IRCCS-Casa Sollievo della Sofferenza, Viale Cappuccini 1, 71013 San Giovanni Rotondo, Italy. *E-mail address:* m.castori@operapadrepio.it

Affiliations are at the end of the document.

doi: https://doi.org/10.1016/j.gim.2021.10.009

Introduction

TAB2 (OMIM *605101) maps to 6q25.1. and encodes for 1 of the 3 proteins (TAB1, TAB2, and TAB3) that intracellularly bind to MAP3K7 (also known as TAK1) to form the TAK1–TABs complex. In particular, TAB2 acts as an adapter protein in TAK1 activation by linking TAK1 to TRAF6.[1] Autoubiquitylation of TRAF6 by the interaction with the TGFβ receptors recruits the TAK1–TAB2 complex through the Npl4 zinc-finger domain of TAB2. This triggers the activation of TAK1[2] and the downstream intracellular signaling networks, such as mitogen-activated protein kinase (MAPK)–p38, MKK4, cJNK, and NF-κB pathways.[3] The TAK1–TABs complex is a central player in the signalosome for inflammation, apoptosis, autophagy, and fibrosis. It is also crucial for connective tissue homeostasis and, in particular, extracellular matrix (ECM) biogenesis by stimulating type I/IV collagen and fibronectin production in mesangial cells and fibroblasts.[4-8]

In 2010, haploinsufficiency of *TAB2* owing to 6q25.1 microdeletions was described in association with congenital heart defects (CHDs) (OMIM 614980).[9] Subsequently, Cheng et al[10] refined the phenotype associated with 6q25.1 microdeletions by reporting 13 new individuals from 7 families. This condition emerged as a multisystem disorder featuring CHD, cardiomyopathy, short stature/growth delay, hypotonia, intellectual disability/developmental delay, facial dysmorphism, and variable connective tissue abnormalities.[10] However, the clinical variability of 6q25.1 microdeletion syndrome remains wide because it ranges from isolated, familial CHD[11] to syndromic presentations resembling Ehlers-Danlos syndrome (EDS) and/or Loeys-Dietz syndrome.[10,12,13]

More rarely, *TAB2* single-nucleotide variants or indel variants were identified for different phenotypes. The p.(Glu569Lys) and p.(Gln540Arg) variants were identified in 2 cases of frontometaphyseal dysplasia type 3. These missense changes likely cause the disease by exerting a gain-of-function effect.[14,15] In total, 6 isolated reports describe heterozygous truncating variants in *TAB2* associated with apparently different phenotypes. In particular, 1 frameshift and 3 nonsense variants were described in association with polyvalvular heart disease with or without additional ocular, craniofacial, and connective tissue anomalies.[16-19] Another family carrying the p.(Thr467Tyrfs*6) variant showed a multisystem disorder resembling a hereditary connective tissue disorder.[13] Finally, the p.(Arg546Ter) variant was reported in a fetus with hypoplasia of the mitral valve, left ventricle, and ascending aorta.[20] Taken together, these observations predict the existence of a phenotypically distinguishable subset of individuals with heterozygous loss-of-function variants in *TAB2*.

In this study, we report a series of 12 individuals from 9 families with loss-of-function variants in *TAB2* and a multisystem phenotype. This condition emerges as a novel recognizable syndrome with cardiovascular anomalies, facial dysmorphisms, and multiple connective tissue features.

Materials and Methods

Patient enrolment

Subjects were recruited from the routine clinical activities of the involved institutions. All patients except 1 (I12, see later) underwent molecular testing for a suspicion of EDS or a related connective tissue disorder. The diagnosis was resolved molecularly by next-generation sequencing (NGS) technologies with a multigene panel, clinical exome, exome sequencing, or genome sequencing (GS) approaches.

Molecular analysis

After DNA extraction and quantification following standard procedures, I1-11 underwent molecular analysis by NGS technologies at the involved institutions following different diagnostic flowcharts. NGS analysis was first carried out in index cases (I1, I2, I3, I6, I7, I8, I9, and I10) and subsequently extended to parents and additional affected relatives, if available. Individuals I2, I3, I7, and I10 were analyzed by a custom-made multigene panel and I1 was analyzed by a clinical exome panel, while I6, I8, and I9 were analyzed by exome sequencing (Supplemental Methods). All variants identified by NGS were confirmed by Sanger sequencing and were interpreted according to the rules of the American College of Medical Genetics and Genomics (Supplemental Methods). In I12, the microdeletion spanning *TAB2* exons 1 to 3 (see Results section) was identified by GS and subsequently confirmed by the revision of the data from a previous comparative genome hybridization array (Supplemental Methods). All *TAB2* variants reported in this study refer to the same reference sequence: NM_015093.

Cell cultures

Primary dermal fibroblasts were obtained from skin biopsies of 6 affected individuals, 2 carrying the previously published p.(Thr467Tyrfs*6) variant[13] and 4 carrying the novel p.(Thr297Ala), p.(Arg441*), p.(Gln504*), and p.(Leu506Serfs*6) variants (I4, I6, I9, and I10, respectively), and of 5 unaffected controls. Fibroblasts were then cultured in Dulbecco's Modified Eagle Medium/Nutrient Mixture F-12 (DMEM-F12) (Thermo Fisher Scientific) plus 10% fetal bovine serum (FBS) (Thermo Fisher Scientific) and 1% penicillin and streptomycin (P/S, 100 U/mL and 100 μg/mL, respectively) (Thermo Fisher Scientific). Primary fibroblast cultures were deposited into the Telethon Genomic and Genetic Disorders Biobank (http://www.operapadrepio.it/ggdbbank/). Human embryonic kidney

(HEK) 293 cell lines were maintained in DMEM with Glutamax supplemented with 10% FBS and 1% P/S. Cell cultures were grown in a 5% carbon dioxide incubator at 37 ºC. All fibroblast cultures were free of mycoplasma.

Generation of expression plasmid

The pCMV-hemagglutinin-(HA)-*TAB2* plasmid was kindly provided by Prof Stephen P. Robertson (University of Otago, Dunedin, New Zealand). The pcDNA3 constructs expressing the HA-tagged *TAB2* variants were generated from HA-tagged *TAB2* wild types by using the QuickChange II Site-Directed Mutagenesis Kit (Stratagene) and a Pfu Taq polymerase (Promega) according to the manufacturer's instructions. The constructs were verified by Sanger sequencing. Primer pairs used are listed in Supplemental Table 1.

Luciferase assay

HEK293 cells were seeded at density of 1.0×10^5 cells/mL per well in a 24-well plate and then transfected with pGL4.32-NF-kB-RE (E849A, Promega) luciferase reporter plasmid together with indicated pcDNA3-HA-TAB2 expression vectors using Lipofectamine LTX (ThermoFisher Scientific) according to the manufacturer's instructions. Renilla luciferase-expressing plasmid (pRL-SV40, Promega) was used to normalize transfection efficiencies. After 48 hours of transfection, cells were lysed in the passive buffer and assayed for both firefly and Renilla luciferase activities using the Dual-GLO Luciferase Assay System (Promega) in a Glomax 96-Well Microplate Luminometer (Promega). Firefly luciferase activity was normalized to Renilla luciferase activity for each transfected well. Values are presented as the mean ± standard error of 3 experimental replicates from 3 independent transfections. To verify whether the cells ectopically expressed the wild-type and all aberrant TAB2, lysates from transfected cells were resolved by electrophoresis on 10% sodium dodecyl-sulfate (SDS) polyacrylamide gel (Biorad), transferred to a nitrocellulose membrane, blocked in gelatin, and then blotted with anti-HA (3724S, Cell Signaling).

Quantification of phosphorylated protein levels

Patients' and controls' fibroblasts were lysed in 1× Dulbecco's phosphate-buffered saline (Thermo Fisher Scientific), 0.025% NP-40, and protease- and phospho-inhibitors (Roche), resolved by electrophoresis on 10% SDS polyacrylamide gel, and transferred to a nitrocellulose membrane. The membranes were blocked in gelatin and then blotted with anti-phospho-TAK1 (9339, Cell Signaling) and anti-GAPDH (sc-47724, Santa Cruz). To analyze the reactive TAK1 phosphorylation level, band intensity of phosphorylated TAK1/GAPDH was quantified using ImageJ software as previously reported.[21]

Osteogenic differentiation

To induce osteogenesis, primary dermal fibroblasts from a previously published subject[13]; individuals I4, I9, and I10; and 3 unaffected controls were plated in cell culture plates at a density of 5×10^4 cells/mL and treated for 28 days with osteogenic medium comprising DMEM-F12 supplemented with 10% FBS , 1% P/S (100 U/ml and 100 µg/mL, respectively), 50 µg/mL ascorbate-2-phosphate (Sigma Aldrich), 10^{-8} M dexamethasone (Sigma Aldrich), and 10^{-2} M β-glycerophosphate (Sigma Aldrich). The presence of calcium deposits in induced cultures was determined by Alizarin Red S (Sigma Aldrich) staining as follows: cells were fixed in 10% formalin (Sigma Aldrich) for 10 minutes, then washed in phosphate-buffered saline without calcium and magnesium (ThermoFisher Scientific), and incubated for 10 minutes at 37 ºC with filtered 2% Alizarin Red S in water. Cells were finally washed several times to remove the excess stain and observed using Axiocam 105 color (Zeiss) connected to Eclipse TE300 Microscope (Nikon). The intensity of the red color in the images was quantified using the ImageJ software (Supplemental Figure 2, Supplemental Methods).[22]

Statistical analysis

Densitometry analysis of immunoblots and osteogenic differentiation-related images were performed using the ImageJ software. Statistical analysis of immunoblotting, luciferase assays, and osteogenic differentiation were performed using unpaired, 2-tailed Student *t* tests with equal variance ($*P < .05$, $**P < .01$, $***P < .001$).

Results

Clinical and molecular data

Eleven individuals (I1-I11) from 8 families (I-VIII) were identified carrying a heterozygous variant in *TAB2*. All variants were private and clustered in a highly conserved TAB2 region encoded by exon 4 (Table 1, Figure 1A, Supplemental Figure 1, Supplemental Results). Seven variants were predicted to be null alleles, whereas a single variant, segregating in 3 variably affected individuals (I3-5), was a missense change (c.889C>T, p.[Thr297Ala]). Individual I12 was heterozygous for a 52 kb microdeletion ([GRCh38] chr6:149308196-149360335/[GRCh37] chr6:149629332-149681471) involving part of *TAB2* (Table 1, Figure 2). This finding was confirmed by re-analysis of the comparative genome hybridization array data performed in 2014 (Supplementary Results). The facial photographs of 8

Table 1 Clinical and molecular data of analyzed individuals

Individual No.	I1	I2	I3	I4	I5	I6	I7	I8	I9	I10	I11	I12
Family	I	II	III	III	III	IV	V	VI	VII	VIII	VIII	IX
Ethnic origin	Finnish	Italian	Italian	Italian	Italian	Belgian	Belgian	Swiss	Swiss	Italian	Italian	Belgian
cDNA change	c.679C>T	c.731del	c.889A>G	c.889A>G	c.889A>G	c.1321C>T	c.1354C>T	c.1385dup	c.1510C>T	c.1516del	c.1516del	NA
Amino acid change	p.(Arg227*)	p.(Pro244Leufs*117)	p.(Thr297Ala)	p.(Thr297Ala)	p.(Thr297Ala)	p.(Arg441*)	p.Arg452*	p.(Tyr462*)	p.(Gln504*)	p.Leu506Serfs*6	p.Leu506Serfs*6	NA
Type of variant	Nonsense	Frameshift	Missense	Missense	Missense	Nonsense	Nonsense	Nonsense	Nonsense	Frameshift	Frameshift	52 kb microdeletion (exons 1-3)
Method of analysis	Clinical exome	Multigene panel	Multigene panel	Segregation	Segregation	ES	Multigene panel	ES	ES	Multigene panel	Segregation	GS
Origin	Sporadic (parents untested)	Familial (parents untested)	Familial	Familial	Familial	De novo	Sporadic (parents untested)	De novo	Familial	Familial	Familial	De novo
Age at examination (y)	28	33	10	44	18	55	58	5	13	29	68	21
Sex	F	M	F	M	F	F	M	F	F	M	F	F
Head circumference (cm) [SD]	54.4 [−0.71]	57 [−0.02]	52 [−0.52]	54.5 [−1.66]	54.5 [−0.62]	54 [−1.03]	54.5 [−1.66]	NA	NA	57 [−0.02]	55.5 [−0.18]	53 [−1.89]
Head circumference (in) [SD][a]	21.4 [−0.71]	22.4 [−0.02]	20.5 [−0.52]	21.5 [−1.66]	21.5 [−0.62]	21.3 [−1.03]	21.5 [−1.66]	NA	NA	22.4 [−0.02]	21.9 [−0.18]	20.9 [−1.89]
Height (cm) [SD]	145 [−3.61]	161.5 [−2.81]	129.5 [−1.75]	176 [−0.68]	159.5 [−1.34]	149.5 [−2.90]	162.5 [-2.65]	109 [−0.42]	163 [+0.50]	164 [−2.43]	154 [−2.20]	160 [−1.27]
Height (in) [SD][a]	57.1 [−3.61]	63.6 [−2.81]	51 [−1.75]	69.3 [−0.68]	62.8 [−1.34]	58.9 [−2.90]	64 [−2.65]	42.9 [−0.42]	64.2 [+0.50]	64.6 [−2.43]	60.6 [−2.20]	63 [−1.27]
Arm span (cm)	146.5	162.5	134	180	160	144.5	165	108	NA	165.3	149.5	156
Arm span (in)	57.7	64	52.8	70.9	63	56.9	65	42.5	NA	65.1	58.9	61.4
Arm span-to-height ratio	1	1	1.03	1.02	1	0.96	1.01	1.00	NA	1	0.97	0.97
Weight (kg) [SD]	45 [−2.11]	58 [−1.52]	28.5 [−0.95]	66 [−0.48]	56.5 [−0.36]	53 [−0.78]	75.4 [+0.47]	18.6 [−0.10]	61 [+1.20]	59.8 [−1.25]	59 [+0.02]	NA
Weight (lb) [SD][a]	99 [−2.11]	129 [−1.52]	63 [−0.95]	145 [−0.48]	125 [−0.36]	117 [−0.78]	166 [+0.47]	41 [−0.10]	134 [+1.20]	132 [−1.25]	130 [+0.02]	NA
Facial features	+	+	+	+	+	+	+	+	+	+	+	+
Long/round face	+	+	+	+	+	+	+	–	+	+	+	+
Wide forehead	+	+	+	+	+	+	+	+	+	+	–	+
Low-set ears	+	+	+	+	+	–	–	–	+	+	–	–
Abnormal eye contour[b]	+	+	+	+	+	+	–	+	+	–	–	+
Prominent nose/columella	–	+	+	+	+	+	+	+	+	+	+	–
Maxillary hypoplasia	+	+	+	–	–	+	+	+	+	+	–	+
Long/smooth lip philtrum	+	+	+	+	–	+	–	–	–	+	+	–
Intraoral Features	+	+	+	–	+	+	–	–	–	+	+	+
Cardiovascular features	+	+	+	+	+	+	+	+	+	+	+	+
ASD/PFO	–	+	–	–	–	–	–	–	–	–	–	–
VSD	–	–	–	–	–	–	–	–	–	–	–	+
Cardiomyopathy	+	+	–	+	–	–	+	–	+	+	–	–
Congestive heart failure	+	–	–	–	–	–	+	–	–	–	–	–
Mitral valve dysplasia/regurgitation	–	–	+	+	+	+	+	+	+	+	+	–
Tricuspid valve dysplasia/regurgitation	–	–	+	+	+	+	–	–	+	+	–	–
Coarctation/stenosis of the aorta	–	–	–	–	–	–	–	–	–	–	+	+
Thoracic aorta/aortic root dilatation	–	–	–	–	–	–	+	–	–	–	–	–
Arrhythmias	–	–	–	+	–	–	+	–	–	+	+	–
Musculoskeletal features	+	+	+	+	+	+	+	+	+	+	+	+
Joint hypermobility (BS)	+ (5/9)	+ (5/9)	+ (7/9)	+ (5/9)	+ (6/9)	+ (5/9)	NA	+ (9/9)	+ (9/9)	+ (5/8)	+	NA
Joint dislocations	+	+	–	–	–	+	–	–	–	+	+	–
Short/webbed neck	+	+	+	+	+	–	+	–	–	+	–	–
Pectus excavatum/carinatum	–	–		+	+	–	–	–	–	–	–	–
Scoliosis	+	+	+	–	+	–	–	–	+	–	+	+

(continued)

Brachydactyly	+	–	–	–	–	+	+	–	–	+	–	+
Long/wide thumbs	+	+	+	+	–	+	–	–	+	–	+	–
Flat feet	+	+	+	–	–	+	–	+	+	+	–	–
Skin features	–	+	+	+	–	+	+	+	+	+	+	–
Soft/velvety/hyperelastic skin	–	+	+	+	–	+	+	+	+	+	+	–
Cutis laxa	–	+	–	–	–	+	–	–	–	+	+	–
Acrogeria	–	+	–	–	–	+	+	–	–	+	+	–
Other features											–	
Hearing loss	–	+	–	–	–	+	+	–	–	–	–	+
Intellectual disability	–	–	–	–	–	–	–	–	–	–	–	–
Chronic pain	+	+	–	–	–	+	–	–	–	–	–	–

ASD, atrial septal defect; *BS*, Beighton score; *ES*, exome sequencing; *F*, female; *GS*, genome sequencing; *M*, male; *NA*, not available; *PFO*, patent forame ovale; *VSD*, ventricular septal defect.

[a]All measurements are expressed in the International System of Units (cm and kg) and Conventional Units (in and lb).

[b]Including almond-shaped eyes, clinical blepharophimosis, downslanting palpebral fissures, and ptosis.

individuals from this study (I1-3, I6, I8-10, I12) (Figure 1B) and of patient 2 and 3 from Ritelli et al[13] were submitted to the Face2Gene CLINIC application to obtain a composite photo (https://www.face2gene.com/). Frequencies of the various facial features according to Face2Gene nomenclature are reported in Figure 1C (https://www.face2gene.com/). All individuals reported in Figure 1B gave their informed consent to publish their clinical photographs.

TAB2 variants alter signaling downstream of TAK1–TAB1 complex

Our previous study highlighted that the *TAB2* c.1398dup variant encodes for a truncated protein that impairs its binding to TAK1, decreases TAK1 autophosphorylation, and alters the activity of the NF-κB and MAPK signaling pathways.[23] All *TAB2* variants identified in this study, except the missense change p.(Thr297Ala), were predicted to generate a truncated protein that lacks the C-terminal zinc finger domain, which is essential for the formation of the TAK1–TAB2 complex. Thus, we hypothesized that the aberrant TAB2 proteins lose their capability to interact with TAK1 complex, which is required for the autophosphorylation-induced activation of TAK1. To explore the functional impact of these novel *TAB2* variants on the TAK1–TABs–dependent pathway, we first quantified the level of phosphorylated TAK1 in cultured skin fibroblasts from 5 affected individuals (1 carrying the previously published p.[Thr467Tyrfs*6] variant[13] and 4 carrying the novel p.[Thr297Ala], p.[Arg441*], p.[Gln504*] and p.[Leu506Serfs*6] variants) and 3 controls. Immunoblot analysis revealed a reduction of TAK1 phosphorylation in all affected subjects when compared with controls (Figure 3A), thus suggesting that TAB2 variants could alter TAK1 activity. To verify whether these *TAB2* variants impair downstream signaling, we performed a luciferase reporter assay that measured a global transcriptional activation by NF-κB signaling as a readout. HEK293 cells were cotransfected with a NF-κB–luciferase reporter plasmid and a vector expressing the wild-type or HA-tagged *TAB2* carrying the nucleotide changes identified in our cohort (the previously reported c.1398dup and the 8 novel variants). We detected a significant 88-fold increase in the luciferase signal in cells expressing wild-type TAB2 when compared with cells transfected with the empty vector (Figure 3B). Accordingly, we did not observe an increase of luciferase transactivation in cells expressing all truncated TAB2 proteins when compared with cells expressing wild-type TAB2 (Figure 3B). Interestingly, cells expressing the TAB2 p.(Thr297Ala) missense variant were able to induce a 55-fold increase of luciferase transactivation when compared with cells with the empty vector (Figure 3B). Immunoblot analysis of whole lysates of HEK293 cells analyzed in the luciferase assay confirms both the ectopic expression of all wild-type and aberrant TAB2 variants and the translational impact of the nucleotide changes (Figure 3B). These data

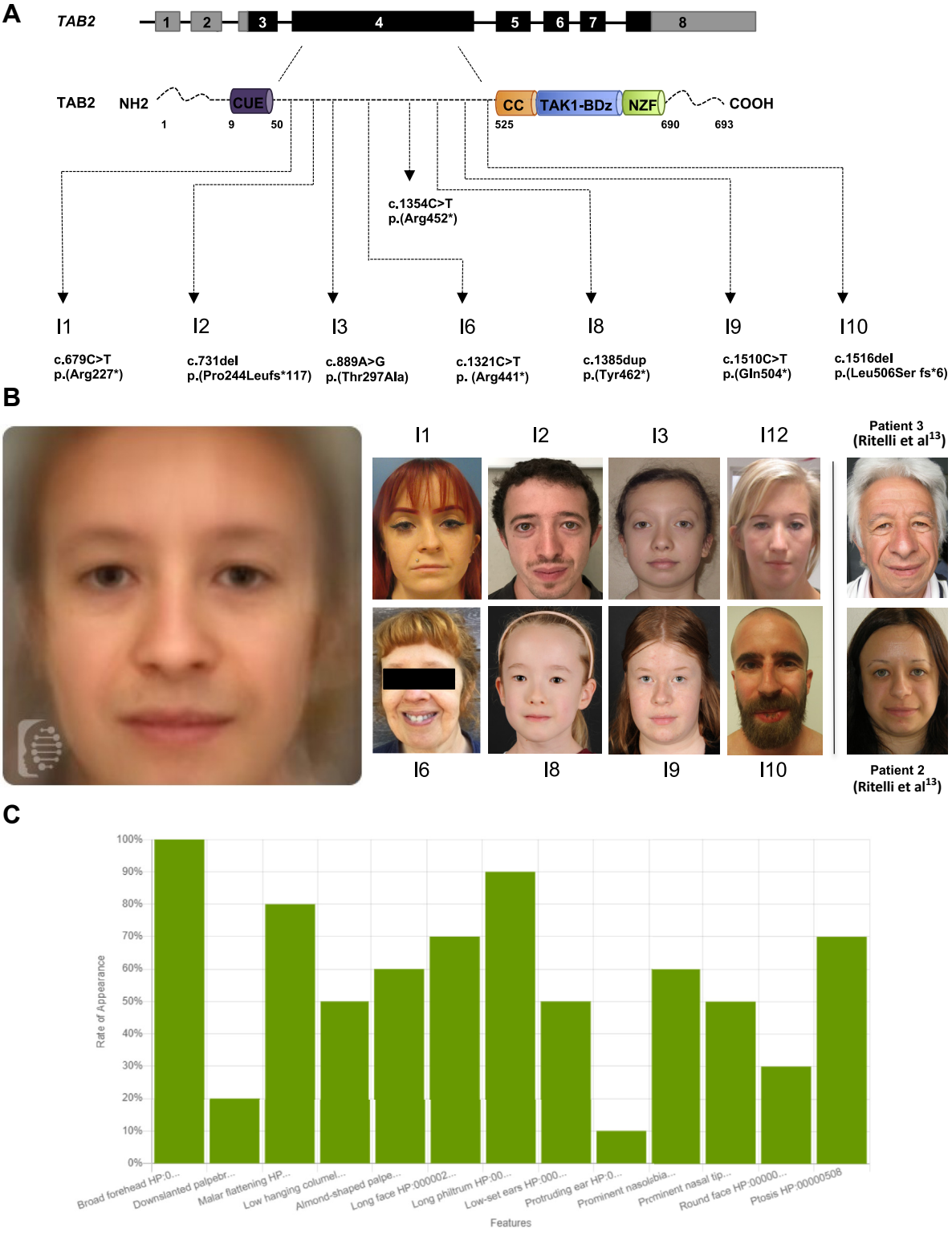

Figure 1 A. Schematic representation of the *TAB2* gene and protein structure. Coding regions are in black and untranslated region sequences are in gray; introns are not to scale. Variants reported here are located on exon 4, which encodes for 35 to 534 amino acids. B. A composite picture of the facial gestalt extracted from the clinical photographs of I1, I2, I3, I6, I8, I9, I10, and I12 (see Figure 2) and those previously published in Ritelli et al[13] (patient 2 and 3) was created by the Face2Gene Research application (https://www.face2gene.com/). C. Frequencies of the reported features in the earlier listed individuals and according to the Face2Gene nomenclature (https://www.face2gene.com/). CC, coiled coil region; CUE, coupling of ubiquitin conjugation to endoplasmic reticulum degradation; NZF, Npl4 zinc finger; TAK1 BD, TAK1 binding domain.

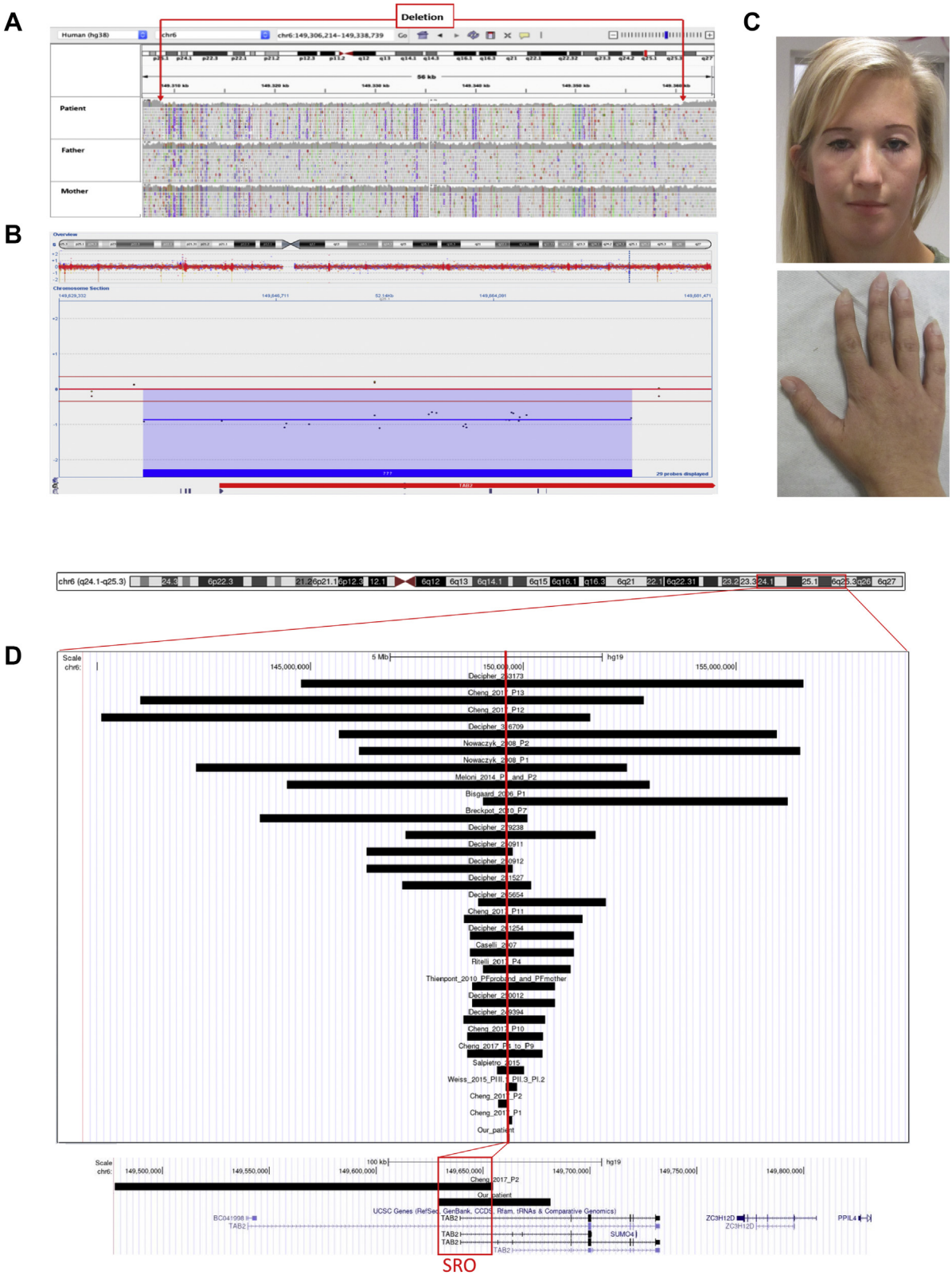

Figure 2 Analysis of the copy number variations in I12 revealing a de novo microdeletion in *TAB2* ([GRCh37] chr6: 149629332-149681471). A. Visualization in integrative genomics viewer shows a loss of coverage in the genome sequencing data of the index in this region but no loss of coverage in the data of I12's father and mother. Breakpoints of the microdeletion are marked by 2 red arrows. B. Array-comparative genomic hybridization results of individual 12. *TAB2* is shown in red. The 52 kb microdeletion overlapping with the 5′ end of *TAB2* in I12 is shown in blue. C. Facial phenotype, including long face, wide forehead, blepharophimosis and midfacial hypoplasia, and brachy-clinodactyly, in I12. D. Comparison of the 6q25.1 microdeletion identified in this patient with previously published cases. E. Detailed view of the SRO (in red) between the patients from 149,629,332 base pair (bp) (centromeric breakpoint in I12) to 149,632,217 bp (telomeric breakpoint in the 249489 Database of Chromosomal Imbalance and Phenotype in Humans using Ensembl Resources patient). Genomic coordinates are based on assembly GRCh37 (hg19). SRO, smallest region of overlap.

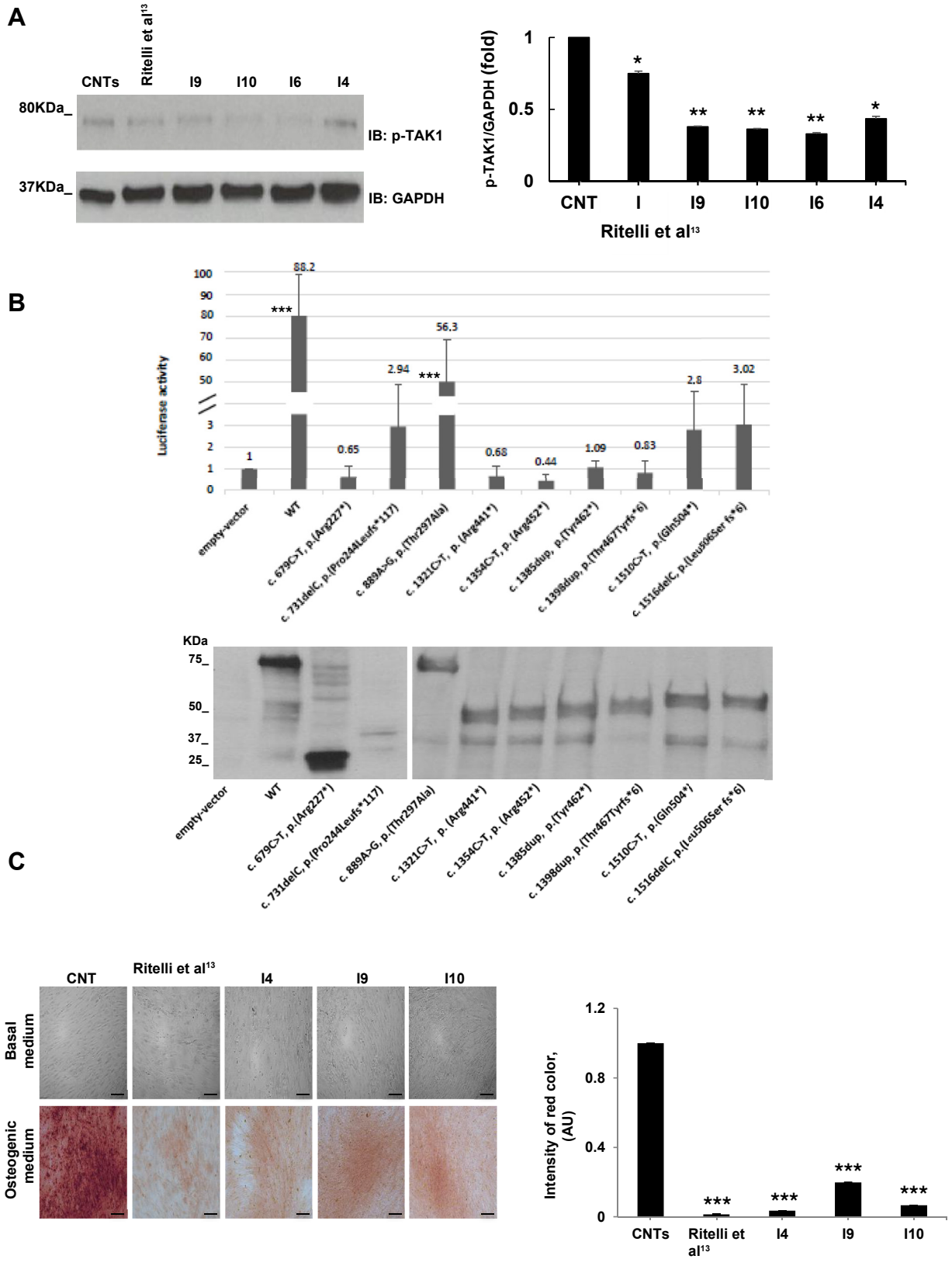

Figure 3 A. Left: total lysates were obtained from indicated individuals and control skin fibroblasts and separated on 10% sodium dodecyl-sulfate polyacrylamide gel and subjected to immunoblotting with the indicated antibodies. Right: levels of phospho-TAK1/GAPDH were quantified by densitometry using ImageJ analysis software. The relative phospho-TAK1/GAPDH levels in control cells were set as 1. Graphs show averages calculated from 3 independent experiments and scale bars represent SEs. Values are expressed as mean ± SEM (**$P < .01$, $n = 3$; *$P < .05$, $n = 3$). B. Up: luciferase assays were performed in human embryonic kidney (HEK) 293 cells cotransfected with a pcDNA3-HA-tagged-TAB2 WT or HA-tagged-altered-TAB2 (as indicated) plasmid, a pGL4.32-NF-kB-RE luciferase reporter plasmid, and a

suggest that all identified *TAB2* variants significantly impair TAK1-TABs mediated signaling.

TAB2 variants compromise osteoblast differentiation

It is well documented that the TAK1–TAB2 complex plays a crucial role in osteoblast differentiation, mineralization, and skeletal development.[24,25] In our cohort, given the high rate of brachydactyly, orthopedic traits, and, to a lesser extent, short stature, we hypothesized that the effects of the deleterious variants were not limited to the nonossified mesodermal derivatives but also extended to the skeletal system. We differentiated primary dermal fibroblasts isolated from 4 affected individuals (1 carrying the previously published p.[Thr467Tyrfs*6] variant[13] and 3 carrying the novel p.[Thr297Ala], p.[Gln504*], and p.[Leu506Serfs*6] variants) and 3 controls. After 28 days of induction, Alizarin Red S staining and calcium content quantification showed a significantly less calcified ECM in patients' cells when compared with control cells (Figure 3C). The differentiation assay was validated by quantifying the expression levels of the osteoblastic marker genes *COL1A1, SPP1, BGLAP, RUNX2,* and *DMP1* at 7, 14, 21, and 28 days from induction in control cells (Supplemental Figure 2, Supplemental Methods). These preliminary data showed that the osteoblast differentiation process from fibroblasts was strongly compromised in affected individuals.

TAB2-related transcriptomic profile

We hypothesized that the dysregulation of TAK1–TAB2–mediated signaling alters the transcriptional profile in different cell types, thus leading to impaired connective tissue homeostasis. To identify potential disease-related pathways and networks, we carried out RNA sequencing (Supplemental Methods) on 6 fibroblast cell lines from 6 affected individuals (2 previously published subjects[13] and individuals I4, I6, I9, and I10). Transcriptome analysis revealed 1567 differentially expressed genes (DEGs) (Supplemental Table 4 sheet 1) with false discovery rate (FDR) < 0.05 (Figure 4A). The expression of 436 DEGs differed significantly with at least a 2.0 log fold change (230 upregulated and 206 downregulated genes). Figure 4A represents the volcano plot that illustrates the statistical significance (FDR) vs fold-change of DEGs. The 436 DEGs formed 16 clusters on the basis of biological processes when querying the Database for Annotation, Visualization, and Integrated Discovery Gene Ontology database with the Functional Annotation clustering Tool (DAVID GO FAT) (Figure 4B and C, Supplemental Table 4 sheet 2) and assuming a threshold of FDR < 0.05 and an enrichment score of 3. These processes are related to cell proliferation, skeletal system development, bone development and homeostasis, regulation of signaling, cardiovascular system development, epithelial cell proliferation, and organ morphogenesis. Figure 4B and C show the most representative biological processes for each cluster.

Discussion

The existence of an under-recognized disorder caused by loss-of-function variants in *TAB2* has been anticipated by the description of the 6q25.1 microdeletion syndrome[10] along with the report of single individuals carrying *TAB2* heterozygous null variants and showing variable congenital birth defects.[13,16-20] The phenotypical convergence between the 6q25.1 microdeletion and specific point variants in *TAB2* was first proposed by our group by comparing a sporadic individual with approximately 2 Mb microdeletion involving *TAB2* and a family with the p.(Thr467Tyrfs*6) variant.[13] Subsequently, we showed that the p.(Thr467Tyrfs*6) variant causes *TAB2* haploinsufficiency.[26]

In this study, we delineated this condition by reporting 12 novel individuals from 9 families of different European ancestries and by exploring their cellular consequences. In 8 families, NGS analysis revealed either a null allele (7 families) or a missense change (1 family) in exon 4 of *TAB2* (Figure 1). All identified variants resulted in either haploinsufficient (null variants) or hypomorphic (missense variant) alleles. In a single case (I12), a 52 kb microdeletion selectively encompassing the first 3 noncoding exons of *TAB2* was identified (Figure 2). The facial and cardiac phenotype observed in I12 was compatible with individuals (I1-11) with single-nucleotide variations or indel variants in *TAB2* (Table 1). Unique features of this subject included underdevelopment of the abdominal mesentery and a wandering spleen owing to underdevelopment of hepatocolic and splenocolic ligaments. Moreover, none of these findings were reported among previously published individuals with 6q25.1 microdeletion syndrome.

pRL-SV40 expressing plasmid. Luciferase activities were normalized to the level of Renilla luciferase. All data are presented as mean ± SEM of the 3 independent experiments. *** $P < .001$ when compared with HA-empty vector. Bottom: to verify the transfection efficiency of the pcDNA3-HA-tagged-TAB2 WT or HA-tagged-altered-TAB2 (as indicated) plasmid in HEK293 cells, an aliquot of the whole protein lysates used in the luciferase assays was separated on 10% sodium dodecyl-sulfate polyacrylamide gel and subjected to immunoblotting with anti-HA antibody. C. Left: Alizarin Red S staining of deposited extracellular matrix derived from cultured control and patient fibroblasts in both basal (upper panel) and osteogenic media (lower panel). Magnification: 10×, scale bar = 100 μm. Osteoblast differentiation was performed for 28 days. Images obtained in 1 of 2 similar experiments are shown. Right: calcium deposition amount in induced osteoblasts was quantified by measuring the intensity of the red color with ImageJ software. All data are presented as mean ± SEM of the 2 independent experiments. ***$P < .001$ compared with control. AU, arbitrary unit; CNT, control; IB, immunoblot; HA, hemagglutinin; p-TAK1, phosphorylated TAK1; WT, wild type.

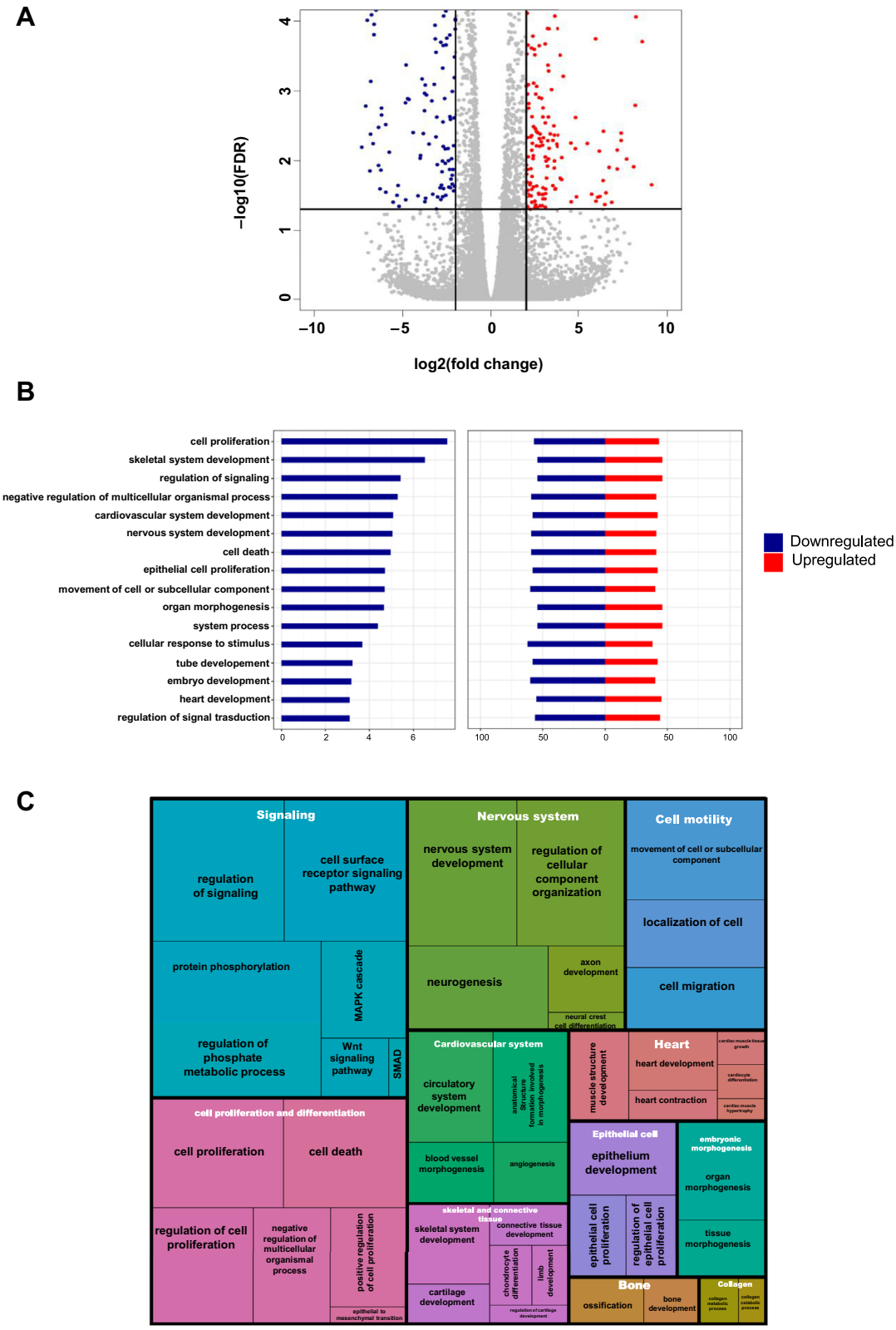

Figure 4 A. Volcano plot showing the 436 differentially expressed genes (blue points represent downregulated genes and red points represent upregulated genes). B. Bar plot (left) showing 16 significantly enriched biological processes, enrichment score > 3; stacked bar plot (right) accounting for proportions of upregulated and downregulated genes for each biological process. C. Treemap representing over-represented biological functions grouped into processes. Sizes of squares are proportional to the number of genes involved in a specific biological process. FDR, false discovery rate; MAPK, mitogen-activated protein kinase.

Syndrome delineation

TAB2 loss-of-function variants (I1-11) results in a different facial morphology, congenital and acquired cardiovascular disease, and musculoskeletal abnormalities (Supplemenatry Table 2). A thorough comparison with previously published patients is hindered by the fragmented extracardiovascular data reported by the authors (Supplemental Table 2). However, the combination of CHD, cardiomyopathy, short stature or growth delay, and facial dysmorphisms (overlapping those observed here) appears to be highly represented in the literature. Hearing loss was an additional low-frequency but clinically relevant manifestation in this series. For this condition, we tentatively propose the term cardio-facial-cutaneous-articular (CFCA) syndrome.

Characteristic facial features are a long and/or round face, a high forehead, almond-shaped eyes/dystopia canthorum, a prominent nose and columella, maxillary hypoplasia, and a long philtrum (Figure 1B and C). This pattern occasionally prompted a suspicion of a RASopathy (I10). Cardiovascular anomalies are present in all but are markedly variable. Mitral and tricuspid valve involvement are most common but clinical severity varies. Cardiomyopathy, mostly of the dilated type, occurred in about half of the patients and was associated with arrhythmias in 4 individuals and congestive heart failure in 2 individuals. Notably, upon follow-up of family 1 harboring the *TAB2* p.(Thr467Tyrfs*6) variant,[13] we learned that patient 3 died from a sudden cardiac death. Moreover, the extended family history was positive for multiple premature deaths in the paternal line.[13] In our present cohort, we did not register any sudden deaths among the evaluated individuals nor their close relatives. Nevertheless, the history of family 1 in Ritelli et al[13] and the progressive nature of myocardial disease in I1 and I7 from the present study suggest that cardiovascular involvement in individuals with *TAB2* loss-of-function variants may be life threatening and warrants cardiac follow-up, even in the absence of CHD. Musculoskeletal and connective tissue involvement frequently includes generalized joint hypermobility with positive Beighton scores (ie, ≥5/8 or ≥5/9) and an abnormal skin texture. Their concurrence, sometimes in combination with joint dislocations and/or chronic pain, aroused a suspicion of a hereditary soft connective tissue disorder, mainly EDS, in 5 families (I1, I2, I3-5, I6, I7, I8, and I9).

The clinical features of *TAB2* loss-of-function variants partially overlap with the cardiospondylocarpofacial syndrome caused by heterozygous variants in *MAP3K7*, encoding TAK1, as evidenced by similar facial characteristics, short stature, and cardiovascular and musculoskeletal anomalies. These similarities were previously observed by our group.[27] Nevertheless, cardiospondylocarpofacial syndrome is clinically characterized by severe functional impairment of the gut and carpal/tarsal synostoses, features not previously reported in *TAB2* deficiency. The existence of overlapping syndromes in the TAK1–TABs complex was also and, for the first time, documented for gain-of-function variants in both *MAP3K7* and *TAB2* in frontometaphyseal dysplasia.[14]

6q25.1 microdeletion syndrome and loss of TAB2 function

Individual I12 was identified by GS, which revealed a microdeletion in *TAB2* (Table 1). She shared many features with I1-11 and patients with 6q25.1 microdeletion syndrome.[10] A comparison between previously published individuals with 6q25.1 microdeletions encompassing *TAB2* and I12 are presented in Figure 2 and Supplemental Table 3. The incidence of CHD, cardiomyopathy, short stature or growth delay, and facial dysmorphisms are comparable among patients with 6q25.1 microdeletions and those with *TAB2* loss-of-function variants. Conversely, joint hypermobility, abnormal skin texture, and intellectual disability/developmental delay showed different rates in patients with 6q25.1 microdeletions and those with *TAB2* loss-of-function variants (Supplemental Table 2 vs Supplemental Table 3). Because individuals with 6q25.1 microdeletions were generally described in more detail, an ascertainment bias might explain the apparent lower rate of extracardiac features in patients with *TAB2* loss-of-function variants, especially of the soft connective tissue abnormalities. However, this likely does not apply to intellectual disability/developmental delay, and therefore, *TAB2* haploinsufficiency alone does not cause neurodevelopmental abnormalities. Accordingly, in 6q25.1 microdeletion syndrome, intellectual disability/developmental delay could be determined by the involvement of neighboring genes. The higher rate of intellectual disability/developmental delay in subjects with larger deletions (Supplemental Table 3) might support this assumption.

Individual I12 allowed refining of the smallest region of overlap of 6q25.1 microdeletion syndrome to approximately 3 kb around the untranslated exon 1 of *TAB2* (Figure 2), and this strongly indicates that the non-neurodevelopmental manifestations are mainly, or even exclusively, caused by *TAB2* perturbations in 6q25.1 microdeletion syndrome. How selectively the deletion of the nontranslated exons in the 5′ region of *TAB2* might affect *TAB2* expression is currently not understood. Loss of key regulatory elements mapped in the deleted sequence, alterations of the 3-dimensional chromatin organization, or the use of alternative start codons may be equally possible mechanisms.

TAB2 identified variants generate either haploinsufficient or hypomorphic alleles

Our study explored the pathogenic effects of 8 novel variants of *TAB2*. In silico findings predicted that 7 *TAB2* variants generate truncated proteins that lack the C-terminal region. The terminal portion of TAB2 is essential for modulating TRAF6-mediated TAK1 activation. This region

contains coiled-coil and TAK1 binding domains that mediate the interaction between TAB2 and TAK1[28] and a zinc finger domain involved in polyubiquitin binding (Figure 1).[29] It is well documented that engineered variants of the zinc finger domain abolish the ability of TAB2 to bind ubiquitin chains and its capability to link the TAK1–TRAF6 complex and then to induce TAK1 activation.[30] At the same time, replacement of the zinc finger domain restores the ability of TAB2 to activate TAK1.[30] Mechanistically, in response to various stimuli, ubiquitinated TRAF6 recruits TAK1 via the C-terminal ubiquitin-binding domain of TAB2, which acts as a scaffold protein.[31] TAB2 transfers the polyubiquitin chains from TRAF6 to TAK1 and then-leads to TAK1 autophosphorylation and downstream signaling activation. Our present and previous[26] results propose *TAB2* loss-of-function variant as a pathological mechanism that negatively impairs the formation of the TRAF6/TAB2/TAK1 signaling complex and, consequently, the regulation of the downstream signaling pathways.

We hypothesized that all TAB2 truncated proteins reported in this study lose the capability to interact with TAK1 and TRAF6 ubiquitinated chains and, in turn, impair TAK1 activation. In vitro studies on patients' fibroblasts and ectopically expressing cells revealed that truncated proteins decrease TAK1 autophosphorylation and alter the activity of NF-κB (Figure 3A and B). Although it is easy to predict the molecular mechanism for the truncated variants, it is not so predictable for the missense p.(Thr297Ala) change. Emerging studies show that the TAK1–TAB2 signaling complex is heavily and dynamically regulated by multiple layers of post-translational modifications. In response to the different stimulations and in a cell type–dependent manner, phosphorylation at Ser372 and Ser524, ubiquitination or methylation at Cys673, sumoylation at Lys329 and Lys562, and O-GlcNAcylation at Thr456 of TAB2 are functionally involved in the activation loop of TAK1-TAB2.[32,33]

We predicted that the single missense p.(Thr297Ala) variant alters a threonine phosphorylation site at residue 297 of TAB2 (Supplemental Figure 3) and, in turn, perturbs TAB2 activity and the TAK1–TAB2 signaling complex. Our functional studies on this variant suggest a possible impact of this amino acid change on TAK1 activation. Indeed, biochemical studies carried out on fibroblasts with the p.(Thr297Ala) change and ectopically expressing cells showed that this variant also reduceds TAK1 phosphorylation and NF-κB activity (Figure 3A and B). However, little is still known about the TAB2 phosphorylation/dephosphorylation mechanics, and further studies are needed to understand its dynamic regulation in both physiological and pathological conditions.

Osteoblast differentiation and transcriptome analyses recapitulate disease manifestations

CFCA syndrome emerges as a multisystem connective tissue disorder with common cardiovascular manifestations and a peculiar face. This implies a pleiotropic nature of the disorder, which reflects the simultaneous perturbation of different morphologic pathways under the influences of *TAB2*. Brachydactyly, joint hypermobility and instability, and short stature indicate major involvement of the musculoskeletal system, and osteoblasts are key cells regulating its functions. We explored the consequences of TAB2-dependent TAK1 dysregulation on fibroblast to osteoblast differentiation.[34] Our investigations showed that patients' fibroblasts differentiated into osteoblasts produced much less calcified ECM than control cells (Figure 3C). This suggests that a defective osteoblast differentiation may underlie the skeletal phenotype.

The observed osteoblast differentiation defect was also supported by transcriptome analysis data, which indicated perturbation of different pathways involved in bone development and homeostasis. Transcriptome analysis further corroborated the master role of *TAB2* in a multitude of cell functions and could help to support genotype–phenotype correlations in CFCA syndrome. For example, the massive deregulation of multiple TGFβ pathway components upstream of the TAK1–TABs complex and other TGFβ canonical and noncanonical components may explain the highly penetrant but extremely diverse cardiac anomalies, spanning from septal defects to single-valve and polyvalvular disease to cardiomyopathy with or without arrhythmias. Facial involvement in CFCA syndrome might be caused by the deleterious influence of *TAB2* loss-of-function variants on the formation and/or migration of neural crest derivatives. Accordingly, transcriptomic analysis showed marked derangement of Wnt signaling, which is a master regulator of neural crest morphogenesis. The facial characteristics of CFCA syndrome may occasionally evoke a clinical diagnosis of a RASopathy. In accordance, transcriptome analysis of *TAB2* cell lines also indicated dysregulation of multiple components of the RAS-MAPK signaling pathway.

Conclusion

Here, we reported the clinical, molecular, and cellular delineation of a recognizable syndrome with cardiovascular, facial, and connective tissue anomalies caused by heterozygous loss-of-function variants in *TAB2*. CFCA syndrome recapitulates the nonneurodevelopmental manifestations of the 6q25.1 microdeletion syndrome and shows the key role of *TAB2* downregulation in determining pleiotropic features in humans. In our experience, major differential diagnoses of CFCA fall in the group of hereditary connective tissue disorders, mainly EDS and TGFβ-pathies, and RASopathies. The available data on natural history and clinical variability of CFCA syndrome indicate the need for a clinical pathway focused on biannual (children) or annual (adults) monitoring and prevention of cardiovascular (ie, dilated cardiomyopathy, arrhythmias, thoracic aorta abnormalities, progressive polyvalvular disease), musculoskeletal

(ie, dislocations, pain), and auditory (ie, hearing loss) complications. Further observations will help to refine the clinical boundaries of CFCA syndrome and the related patients' needs to set up a personalized management program.

Data Availability

For next-generation sequencing analysis, multigene panel for I2, I3-5, I7, I10-11, clinical and exome sequencing for I1, I6, I8, I9, genome sequencing for I12, and genomic array analysis for I12, raw experimental data are available upon request. RNA sequencing data were deposited in GEO NCBI and are available at https://www.ncbi.nlm.nih.gov/geo/query/acc.cgi?acc=GSE180329.

Acknowledgments

The authors thank Dr Lucio Difilippo (Next Generation Diagnostics srl) for his technical support in RNA sequencing and Dr Giovanna Traficante for performing a skin biopsy on individual I10. The authors thank Prof Stephen P. Robertson (University of Otago, Dunedine, New Zealand) for kindly providing the pCMV-HA-TAB2 plasmid.

This project was funded by the Italian Ministry of Health Ricerca Corrente 2018-21 (to L.M. and M.C.) and the Regione Puglia. J.B. and B.C. are supported by a Senior Clinical Investigator fellowship of the Fonds voor Wetenschappelijk Onderzoek (FWO) Flanders. C.G. and M.R. were supported by the Swiss National Science Foundation (31003A-173183). B.C. was supported by a Junior grant from the Research Foundation—Flanders (G035620N). D.C. was supported by Fondazione Telethon Core Grant, Armenise-Harvard Foundation Career Development Award, European Research Council (grant agreement 759154, CellKarma), and the Rita-Levi Montalcini program from MIUR.

Author Information

Conceptualization: L.M., M.C., S.M.; Data Curation: L.M., M.C., S.M., A.Carb., A.Cari.; Formal Analysis: L.M., A.Carb., A.Cari.; Funding Acquisition: L.M., M.C., B.C., D.C., J.B.; Investigation: L.M., C.F., A.Carb., A.Cari.; Methodology: G.N., C.F., A.S., F.R., O.P., G.F.; Resources: C.F., G.N., A.S., Software: A.Cari., D.C.; Supervision: M.C.; Validation: G.N., A.C.; O.P.; Writing-original draft: M.C., L.M., S.M., A.C., A.C.; Writing-review and editing: J.B., C.D.L., A.F., C.G., P.G., M.K.H., G.M., H.V.E., B.C., M.R.

Ethics Declaration

This study was conducted in accordance with the 1984 Helsinki declaration and its subsequent versions and received Institutional Review Board approval from the Fondazione IRCCS-Casa Sollievo della Sofferenza (approval no. 2021/13/CE). All enrolled affected individuals and available unaffected relatives/parents signed an informed consent form for research use of their molecular, cellular, and clinical data. All individuals reported in Figure 1B gave their informed consent to publish their clinical photographs.

Conflict of Interest

The authors declare no conflict of interest related to this article. D.C. is the founder and shareholder of and consultant for Next Generation Diagnostics srl. Some of the authors of this publication are members of the European Reference Network for Intellectual Disability, Telehealth, Autism and Congenital Anomalies (ERN-ITHACA) (EU Framework Partnership Agreement ID: 3HP-HP-FPA ERN-01-2016/739516). J.B. and B.C. are senior clinical investigators for the Research Foundation—Flanders. B.C. is member of the European Reference Network on Rare Skin Disorders (ERN-SKIN). A.F. is member of the European Reference Network on Rare and Complex Connective Tissue and Muscoloskeletal Diseases (ERN-ReCONNET).

Additional Information

The online version of this article (https://doi.org/10.1016/j.gim.2021.10.009) contains supplementary material, which is available to authorized users.

Affiliations

[1]Division of Medical Genetics, Fondazione IRCCS-Casa Sollievo della Sofferenza, San Giovanni Rotondo, Italy; [2]Unit of Chronobiology, Division of Internal Medicine, Fondazione IRCCS-Casa Sollievo della Sofferenza, San Giovanni Rotondo, Italy; [3]Institute for Applied Mathematics "Mauro Picone" National Research Council, Naples, Italy; [4]Center for Human Genetics, University Hospital Leuven, Leuven, Belgium; [5]Laboratory of Medical Genetics, Department of Molecular Medicine, Sapienza University, San Camillo-Forlanini Hospital, Rome, Italy; [6]Division of Metabolism and Children's Research Center, University Children's Hospital Zurich and University of Zurich, Zurich, Switzerland; [7]Department of Clinical Genetics and Genomics, Turku University Hospital and University of Turku, Turku, Finland; [8]Medical Genetics Unit, Meyer Children's University Hospital, Florence, Italy; [9]Medical Genetics Unit, University of Florence, Florence, Italy; [10]Telethon Institute of Genetics and Medicine (TIGEM), Naples, Italy; [11]Department of Translational Medicine, University of Naples "Federico II", Naples, Italy; [12]Center

for Medical Genetics and Department of Biomolecular Medicine, Ghent University Hospital, Ghent, Belgium

References

1. Walsh MC, Kim GK, Maurizio PL, Molnar EE, Choi Y. TRAF6 autoubiquitination-independent activation of the NFkappaB and MAPK pathways in response to IL-1 and RANKL. *PLOS ONE*. 2008;3(12):e4064. http://doi.org/10.1371/journal.pone.0004064.
2. Sorrentino A, Thakur N, Grimsby S, et al. The type I TGF-beta receptor engages TRAF6 to activate TAK1 in a receptor kinase-independent manner. *Nat Cell Biol*. 2008;10(10):1199–1207. http://doi.org/10.1038/ncb1780.
3. Kim SY, Shim JH, Chun E, Lee KY. Reciprocal inhibition between the transforming growth factor-β-activated kinase 1 (TAK1) and apoptosis signal-regulating kinase 1 (ASK1) mitogen-activated protein kinase kinase kinases and its suppression by TAK1-binding protein 2 (TAB2), an adapter protein for TAK1. *J Biol Chem*. 2012;287(5):3381–3391. http://doi.org/10.1074/jbc.M111.317875.
4. Chin BY, Mohsenin A, Li SX, Choi AM, Choi ME. Stimulation of pro-alpha(1)(I) collagen by TGF-beta(1) in mesangial cells: role of the p38 MAPK pathway. *Am J Physiol Renal Physiol*. 2001;280(3):F495–F504. Published correction appears in *Am J Physiol Renal Physiol*. 2020;319(6):F1000. https://doi.org/10.1152/ajprenal.2001.280.3.F495.
5. Wang C, Deng L, Hong M, Akkaraju GR, Inoue J, Chen ZJ. TAK1 is a ubiquitin-dependent kinase of MKK and IKK. *Nature*. 2001;412(6844):346–351. http://doi.org/10.1038/35085597.
6. Ono K, Ohtomo T, Ninomiya-Tsuji J, Tsuchiya M. A dominant negative TAK1 inhibits cellular fibrotic responses induced by TGF-beta. *Biochem Biophys Res Commun*. 2003;307(2):332–337. http://doi.org/10.1016/s0006-291x(03)01207-5.
7. Hocevar BA, Prunier C, Howe PH. Disabled-2 (Dab2) mediates transforming growth factor beta (TGFbeta)-stimulated fibronectin synthesis through TGFbeta-activated kinase 1 and activation of the JNK pathway. *J Biol Chem*. 2005;280(27):25920–25927. http://doi.org/10.1074/jbc.M501150200.
8. Kim CB. MAPK-ing out the pathways in lung stem cell regulation. *Cell Stem Cell*. 2007;1(1):11–13. http://doi.org/10.1016/j.stem.2007.05.007.
9. Thienpont B, Zhang L, Postma AV, et al. Haploinsufficiency of TAB2 causes congenital heart defects in humans. *Am J Hum Genet*. 2010;86(6):839–849. http://doi.org/10.1016/j.ajhg.2010.04.011.
10. Cheng A, Dinulos MBP, Neufeld-Kaiser W, et al. 6q25.1 (TAB2) microdeletion syndrome: congenital heart defects and cardiomyopathy. *Am J Med Genet A*. 2017;173(7):1848–1857. http://doi.org/10.1002/ajmg.a.38254.
11. Weiss K, Applegate C, Wang T, Batista DA. Familial TAB2 microdeletion and congenital heart defects including unusual valve dysplasia and tetralogy of fallot. *Am J Med Genet A*. 2015;167A(11):2702–2706. http://doi.org/10.1002/ajmg.a.37210.
12. Salpietro V, Ruggieri M, Mankad K, et al. A de novo 0.63 Mb 6q25.1 deletion associated with growth failure, congenital heart defect, underdeveloped cerebellar vermis, abnormal cutaneous elasticity and joint laxity. *Am J Med Genet A*. 2015;167A(9):2042–2051. http://doi.org/10.1002/ajmg.a.37118.
13. Ritelli M, Morlino S, Giacopuzzi E, et al. A recognizable systemic connective tissue disorder with polyvalvular heart dystrophy and dysmorphism associated with TAB2 mutations. *Clin Genet*. 2018;93(1):126–133. http://doi.org/10.1111/cge.13032.
14. Wade EM, Daniel PB, Jenkins ZA, et al. Mutations in MAP3K7 that alter the activity of the TAK1 signaling complex cause frontometaphyseal dysplasia. *Am J Hum Genet*. 2016;99(2):392–406. http://doi.org/10.1016/j.ajhg.2016.05.024.
15. Wade EM, Jenkins ZA, Daniel PB, et al. Autosomal dominant frontometaphyseal dysplasia: delineation of the clinical phenotype. *Am J Med Genet A*. 2017;173(7):1739–1746. http://doi.org/10.1002/ajmg.a.38267.
16. Ackerman JP, Smestad JA, Tester DJ, et al. Whole exome sequencing, familial genomic triangulation, and systems biology converge to identify a novel nonsense mutation in TAB2-encoded TGF-beta activated kinase 1 in a child with polyvalvular syndrome. *Congenit Heart Dis*. 2016;11(5):452–461. http://doi.org/10.1111/chd.12400.
17. Caulfield TR, Richter JE Jr, Brown EE, Mohammad AN, Judge DP, Atwal PS. Protein molecular modeling techniques investigating novel TAB2 variant R347X causing cardiomyopathy and congenital heart defects in multigenerational family. *Mol Genet Genomic Med*. 2018;6(4):666–672. http://doi.org/10.1002/mgg3.401.
18. Chen J, Yuan H, Xie K, et al. A novel TAB2 nonsense mutation (p.S149X) causing autosomal dominant congenital heart defects: a case report of a Chinese family. *BMC Cardiovasc Disord*. 2020;20(1):27. http://doi.org/10.1186/s12872-019-01322-1.
19. Liu H, Giguet-Valard AG, Simonet T, et al. Next-generation sequencing in a series of 80 fetuses with complex cardiac malformations and/or heterotaxy. *Hum Mutat*. 2020;41(12):2167–2178. http://doi.org/10.1002/humu.24132.
20. Permanyer E, Laurie S, Blasco-Lucas A, et al. A single nucleotide deletion resulting in a frameshift in exon 4 of TAB2 is associated with a polyvalular syndrome. *Eur J Med Genet*. 2020;63(4):103854. http://doi.org/10.1016/j.ejmg.2020.103854.
21. Micale L, Morlino S, Biagini T, et al. Insights into the molecular pathogenesis of cardiospondylocarpofacial syndrome: MAP3K7 c.737-7A > G variant alters the TGFβ-mediated α-SMA cytoskeleton assembly and autophagy. *Biochim Biophys Acta Mol Basis Dis*. 2020;1866(6):165742. http://doi.org/10.1016/j.bbadis.2020.165742.
22. Camci-Unal G, Laromaine A, Hong E, Derda R, Whitesides GM. Biomineralization guided by paper templates. *Sci Rep*. 2016;6(1):27693. http://doi.org/10.1038/srep27693.
23. Robinson MD, Oshlack A. A scaling normalization method for differential expression analysis of RNA-seq data. *Genome Biol*. 2010;11(3):R25. http://doi.org/10.1186/gb-2010-11-3-r25.
24. Yang H, Guo Y, Wang D, Yang X, Ha C. Effect of TAK1 on osteogenic differentiation of mesenchymal stem cells by regulating BMP-2 via Wnt/β-catenin and MAPK pathway. *Organogenesis*. 2018;14(1):36–45. http://doi.org/10.1080/15476278.2018.1455010.
25. Kim K, Kim JH, Kim I, Seong S, Kim N. TRIM38 regulates NF-κB activation through TAB2 degradation in osteoclast and osteoblast differentiation. *Bone*. 2018;113:17–28. http://doi.org/10.1016/j.bone.2018.05.009.
26. Morlino S, Carbone A, Ritelli M, et al. TAB2 c.1398dup variant leads to haploinsufficiency and impairs extracellular matrix homeostasis. *Hum Mutat*. 2019;40(10):1886–1898. http://doi.org/10.1002/humu.23834.
27. Morlino S, Castori M, Dordoni C, et al. A novel MAP3K7 splice mutation causes cardiospondylocarpofacial syndrome with features of hereditary connective tissue disorder. *Eur J Hum Genet*. 2018;26(4):582–586. http://doi.org/10.1038/s41431-017-0079-x.
28. Takaesu G, Kishida S, Hiyama A, et al. TAB2, a novel adaptor protein, mediates activation of TAK1 MAPKKK by linking TAK1 to TRAF6 in the IL-1 signal transduction pathway. *Mol Cell*. 2000;5(4):649–658. http://doi.org/10.1016/s1097-2765(00)80244-0.
29. Li Y, Okatsu K, Fukai S, Sato Y. Structural basis for specific recognition of K6-linked polyubiquitin chains by the TAB2 NZF domain. *Biophys J*. 2021;120(16):3355–3362. http://doi.org/10.1016/j.bpj.2021.06.037.
30. Kanayama A, Seth RB, Sun L, et al. TAB2 and TAB3 activate the NF-kappaB pathway through binding to polyubiquitin chains. *Mol Cell*. 2004;15(4):535–548. http://doi.org/10.1016/j.molcel.2004.08.008.
31. Sato Y, Yoshikawa A, Yamashita M, Yamagata A, Fukai S. Structural basis for specific recognition of Lys 63-linked polyubiquitin chains by NZF domains of TAB2 and TAB3. *EMBO J*. 2009;28(24):3903–3909. http://doi.org/10.1038/emboj.2009.345.
32. Hirata Y, Takahashi M, Morishita T, Noguchi T, Matsuzawa A. Post-translational modifications of the TAK1-TAB complex. *Int J Mol Sci*. 2017;18(1):205. http://doi.org/10.3390/ijms18010205.

33. Gu Z, Chen X, Yang W, et al. The SUMOylation of TAB2 mediated by TRIM60 inhibits MAPK/NF-κB activation and the innate immune response. *Cell Mol Immunol.* 2021;18(8):1981–1994. http://doi.org/10.1038/s41423-020-00564-w.

34. Jiang S, Wu Y, Wu S, et al. Silencing TAK1 reduces MAPKs-MMP2/9 expression to reduce inflammation-driven neurohistological disruption post spinal cord injury. *Cell Death Discov*. 2021;7(1):96. http://doi.org/10.1038/s41420-021-00481-5.